Open Ceramics 9 (2022) 100243

Contents lists available at ScienceDirect

Open Ceramics

journal homepage: www.sciencedirect.com/journal/open-ceramics

Cork derived TiO_2 biomorphic ecoceramics

Robert C. Pullar [a,c,*], Anais Accaries [b], Dimitri G.H. Scheffer [b], Ana P.F. Caetano [a], Rui M. Novais [a]

[a] Department of Materials and Ceramic Engineering/CICECO-Aveiro Institute of Materials,University of Aveiro, Campus Universitário de Santiago, 3810-193, Aveiro, Portugal

[b] L'École d'ingénieurs ENSIL-ENSCI, University of Limoges, Campus Ester, Parc Ester Technopole, 16 Rue Atlantis, 87280, Limoges, France

[c] Department of Molecular Sciences and Nanosystems (DSMN), Ca' Foscari University of Venice, Scientific Campus, Via Torino 155, 30172, Venezia Mestre, VE, Italy

ARTICLE INFO

Keywords:
Titania
Cork
Biomorphic ceramics
Ecoceramics
Photocatalysis

ABSTRACT

Environmentally conscious biomorphic ceramics (Ecoceramics) are a new class of material manufactured from renewable resources and wastes. Sustainable cork wastes were pyrolysed, and this activated carbon template infiltrated with a sol-gel precursor (from aqueous green-chemistry) to form TiO_2 on heating in air, with the honeycomb microstructure of cork. Physical and optical band gap properties were characterised by XRD, SEM and Raman and UV–vis spectroscopy, and differences between alkaline and acidic activation of the carbon template also studied. With activation by HCl, HNO_3 or H_2SO_4, a mixture of anatase and rutile formed. NaOH activation resulted in pure anatase, but a large amount of Na was retained. At 1000 °C acid activated ecoceramics formed pure rutile, but the NaOH activated one formed $Na_2Ti_6O_{13}$ (sodium hexatitanate) as the major phase, coexisting with anatase, brookite and rutile. This material is worth further investigation, as $Na_2Ti_6O_{13}$ is reported as a photocatalyst in its own right.

1. Introduction

TiO_2 is an economic, non-toxic semiconductor with a band gap (Eg) in the UV–visible region [1], and has been a well-known photocatalyst since the 1970's [2,3]. TiO_2 combats pollution via a photo-induced reaction occurring at the photocatalyst's surface. Absorption of a photon with energy >Eg Ref. [4] makes electron-hole pairs that create radicals able to reduce organic or inorganic matter, and inactivate/kill bacteria [5]. Solar light is ~4% UV and ~46% visible light at sea level, but the most common titania phase used in photocatalysis, anatase, functions only under UV (Eg = 3.23 eV = 384 nm) exploiting just ~4% of solar light [6]. However, the rutile form of TiO_2 works under visible light (Eg = 3.02 eV = 410 nm) [7]. A more efficient photocatalyst exploiting both UV and visible light can produced by combining the two phases; indeed, it was demonstrated that the well-known commercial TiO_2 photocatalyst Degussa/Evonik Aeroxide P25 actually consists of 76 wt% anatase, 11 wt% rutile and 13 wt% amorphous TiO_2 [8].

Plants and wood are natural bio-organic composites, exhibiting porous, anisotropic morphologies, with excellent strength at a low density compared to metals or ceramics [9]. They have a highly porous cellular microstructure, the cells forming a system of channels to carry water. Liquid infiltration techniques can be used to impregnate the cellular structure of wood and transform it into an inorganic copy of the original cellular structure [10]. The wood is first pyrolysed to a pure carbon skeleton which maintains its structure, but is highly nanoporous, and can be impregnated with a solution, which converts to the inorganic phase on heating in air, with loss of the carbon. This can be used as a template for the synthesis of novel inorganic materials with highly anisotropic cellular microstructures, a new class of ceramics now referred to as ecoceramics – environmentally conscious ceramics [11,12]. Although most ecoceramics work has focused on SiC [13], several oxide ecoceramics have been produced from various woods, including TiO_2 from rattan and pine [14]. However, until the pioneering work by Pullar et al. at CICECO/Aveiro University, no ecoceramics had been produced from cork.

Cork is the bark of a slow-growing oak, *Quercus suber* L., with Europe supplying 85% of all cork, and Portugal is the major global producer (50%) [15]. Cork has a 3-DOM microstructure of hollow cells different from other woods, consisting of a hexagonal honeycomb of ~20 μm cells in the radial direction [16], with cell walls 1 μm thick (40M–100 M

* Corresponding author. Department of Materials and Ceramic Engineering/CICECO-Aveiro Institute of Materials, University of Aveiro, Campus Universitário de Santiago, 3810-193, Aveiro, Portugal.

E-mail addresses: robertcarlyle.pullar@unive.it, rpullar@ua.pt (R.C. Pullar).

https://doi.org/10.1016/j.oceram.2022.100243
Received 25 January 2022; Received in revised form 21 February 2022; Accepted 26 February 2022
Available online 1 March 2022

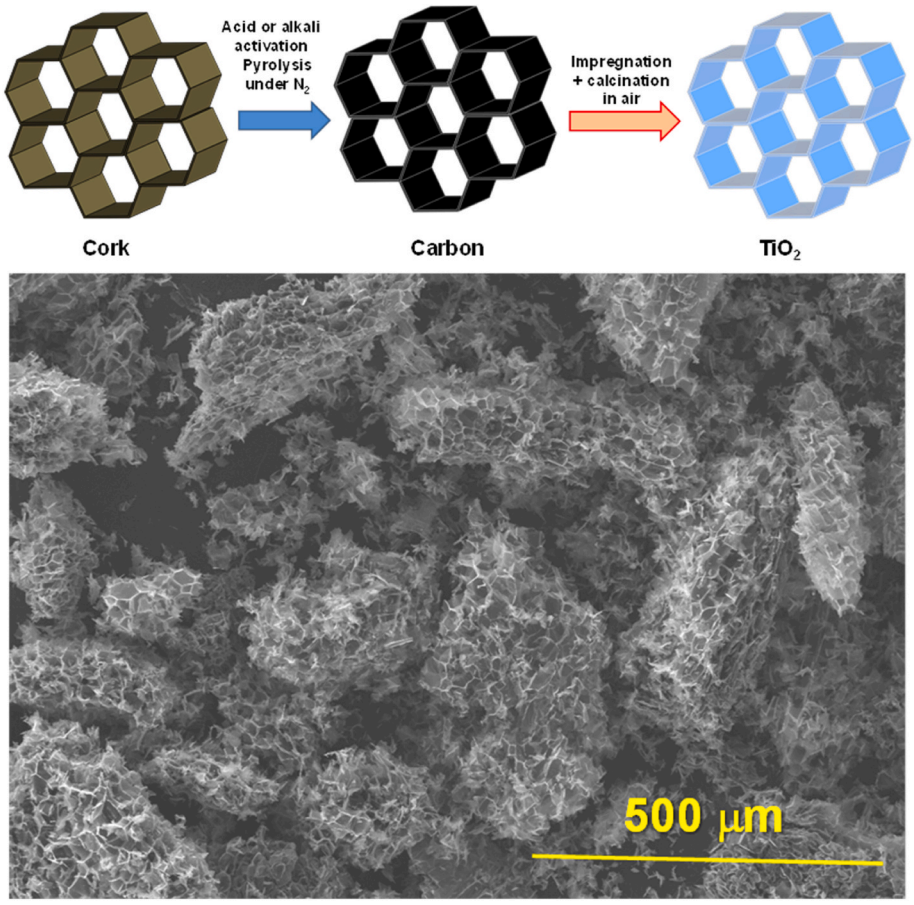

Fig. 1. Scheme of the ecoceramics synthesis process, and an SEM image of the activated and pyrolysed cork powder.

cells/cm^3) [17], and a very low density of 0.12–0.24 g/cm^3 [17]. Cork is a uniquely sustainable and renewable resource, the bark being harvested every 9 years without harming the tree, which lives on as a carbon sink for >200 years [18]. As cork oak trees store carbon in order to regenerate their bark, a harvested cork oak tree absorbs up to 5 times more CO_2 in a lifetime than one that is left alone, and cork can sequester up to 5.7 T CO_2/ha/yr [19]. As such, cork is an ideal natural template for Ecoceramics.

The group at CICECO/Aveiro University was the first to create cork-derived ecoceramics [20], and has reported lightweight magnetic hexaferrite "foams" [21], zinc oxide [22], calcium carbonate [23] and ceria ecoceramics [24], the latter for applications in the thermochemical splitting of water and CO_2 to create hydrogen and CO for renewable fuels using concentrated solar light [25,26]. In this paper we detail the synthesis and characterisation of the first titania ecoceramics derived from cork templates. These were infiltrated with an aqueous sol-gel precursor made by a green chemistry route, also developed by the group at CICECO/Aveiro University [27], and the resulting TiO_2 ecoceramics were characterised by XRD, SEM, and Raman and UV–vis spectroscopy. We also studied and compared the effects of alkaline and acidic activation of the cork-carbon template.

2. Experimental

The cork used was a waste cork powder, supplied by Amorim, obtained after finishing operations during the preparation of cork bottle stoppers. It has a stated particle size of 250–500 μm, and a density of 0.05–0.07 g/cm^3 [28]. The activation solutions used were each 10 M concentration, made from NaOH (ACS reagent, 97%, Sigma Aldrich), HCl (VWR AnalaR, 37%)), HNO_3 (Fluka, 65%) and H_2SO_4 (Sigma Aldrich, reagent grade, 95–98%). Titanium *iso*-propoxide (Aldrich, 97%)) was used to produce the precursor sol, with isopropyl alcohol (propan-2-ol, VWR, GPR Rectapur). Distilled water was used in all cases.

2.1. Activation and pyrolysis of the cork

The pyrolysis and activation process was based on our previous work [20,24,29], but for the first time acids were also used for activation. Cork powder was added to the activating solution and then magnetically stirred at room temperature for 2 h. The solid-to-liquid ratio was kept constant (0.8 g cork/50 mL solution). After filtration (nylon net; PA 15/11 L = 1050) and drying (12 h at 80 °C), the cork was placed in graphite crucibles, and then pyrolysed under nitrogen in a vertical split graphite furnace ref. 319/18 purchased from Thermolab, Portugal. The following cycle was used: i) 5 °C/min heating rate up to 150 °C; (ii) 10 °C/min heating rate up to 900 °C; iii) 30 min dwell time at this temperature; and (iv) cooling (at 10 °C/min) to room temperature. The pyrolysed activated cork was washed with distilled water until neutral pH and dried in the oven at 80 °C.

2.2. Synthesis of the titania precursor sol

The synthesis was based on that in Refs. [27,30,31]. In brief, titanium *iso*-propoxide ($Ti(OCH(CH_3)_2)_4$) was added to isopropyl alcohol (IPA), and then mechanically stirred at 400–600 RPM. To this solution was added dropwise another solution containing an excess of deionised water necessary to hydrolyse the titanium propoxide, 2.5 x that amount of IPA, and HNO_3 to peptise the sol, with a HNO_3:Ti^{4+} ratio of 1:2.5. The resulting thick white precipitate and solution were then placed on a rotary evaporator (Büchi rotavapor R-210) and evaporated to dryness at

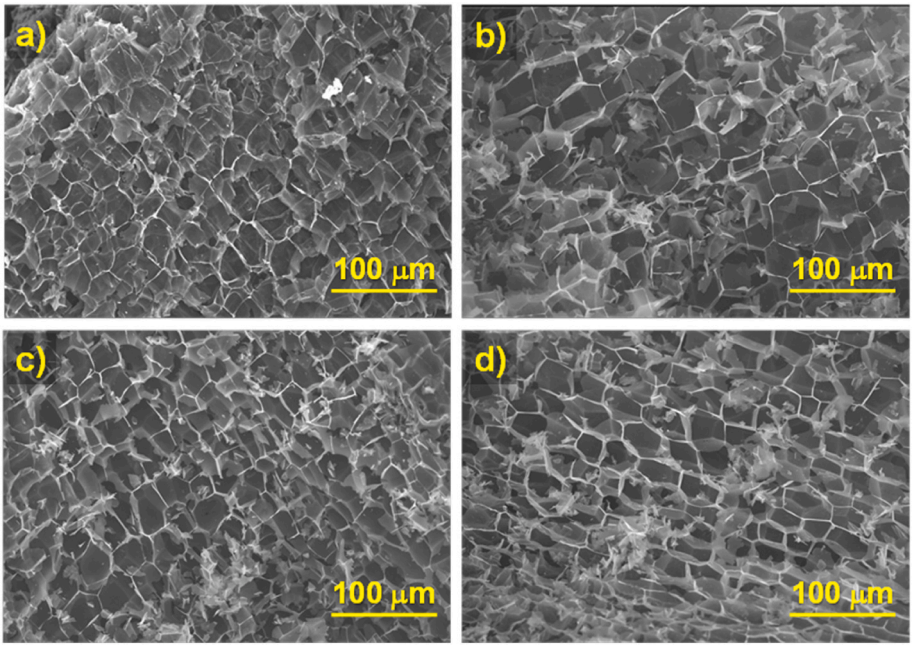

Fig. 2. SEM images of the activated and pyrolysed cork powders, using a) NaOH, b) HCl, c) HNO_3 and d) H_2SO_4 for activation.

55 °C and 100 mbar. Distilled water was added to redisperse the powder, and it was then placed again on the rotary evaporator under 80 mbar and 55 °C. This dried to a yellowish viscous gel. Afterwards distilled water was added again, and the gel dispersed in a few minutes to form an off-white sol with 1 M concentration.

2.3. Ecoceramic synthesis

For impregnation with the titania precursor sol, pyrolysed activated cork powders were placed in the rotary evaporator, the sol added, and then dried at 55 °C and 60 mbar. Once the sol had been evaporated, the cork was dried at 80 °C in an oven for 24 h. The samples were then heated/calcined at two different temperatures in air, 450 °C and

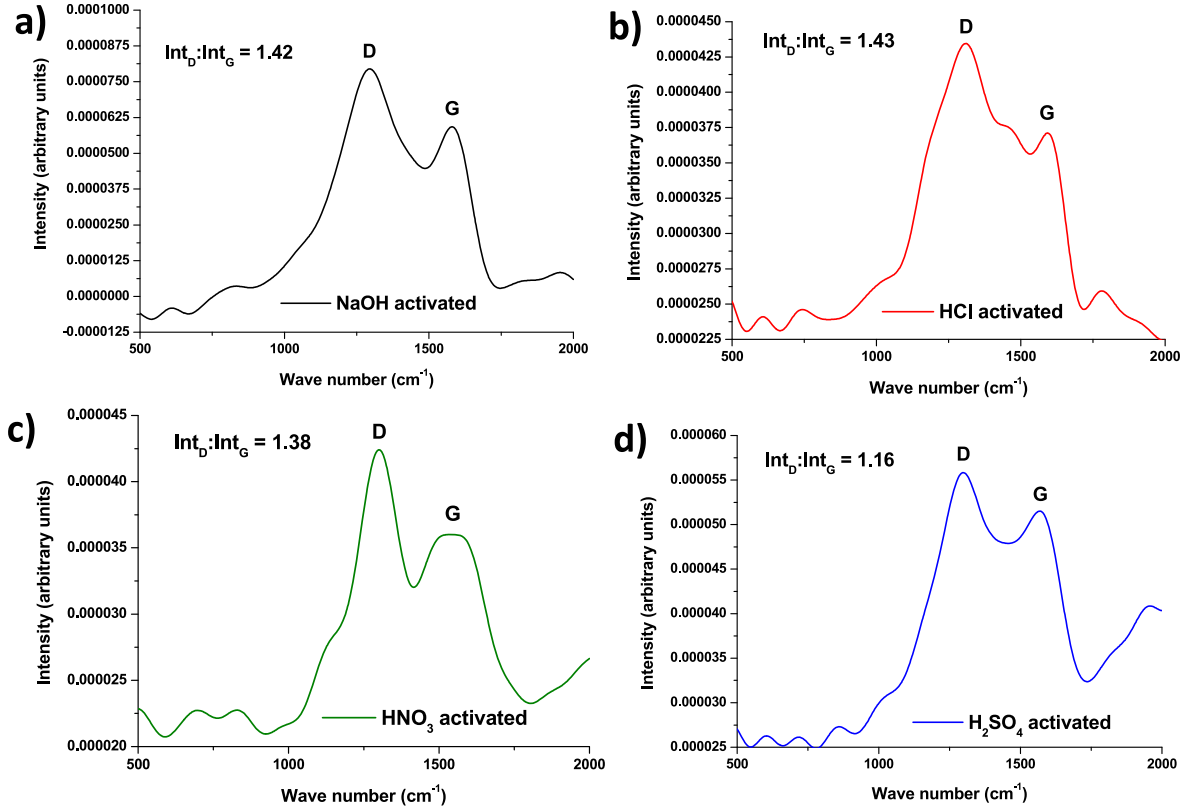

Fig. 3. Raman spectra of the activated and pyrolysed cork powders, using a) NaOH, b) HCl, c) HNO_3 and d) H_2SO_4 for activation. The D:G ratios are shown on each plot.

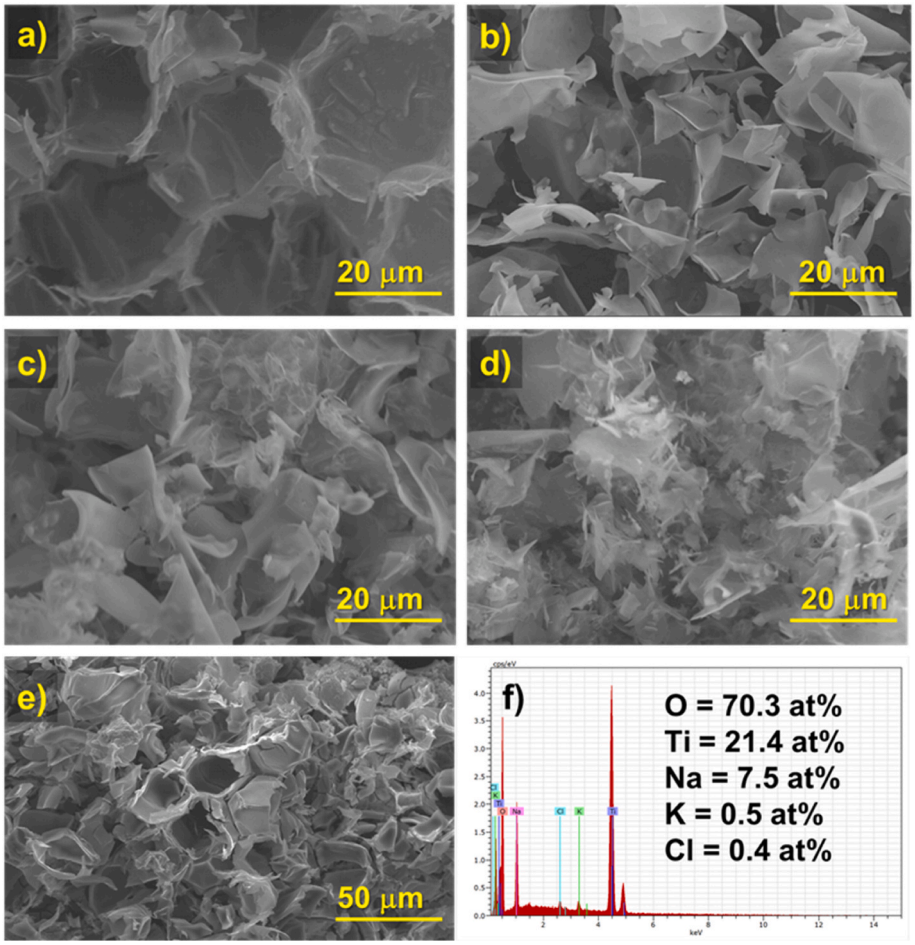

Fig. 4. SEM images of the TiO_2 ecoceramics heated to 450 °C, activated using a) NaOH, b) HCl, c) HNO_3 and d) H_2SO_4. A larger magnification image of the NaOH activated ecoceramic is shown in e), and the EDS spectrum of this sample is shown in f).

1000 °C. The heating conditions were: 1 °C/min from room temperature to the required temperature (450 °C or 1000 °C), 30 min dwell, and cooling at 1 °C/min to room temperature.

2.4. Characterisation

The microstructure of the inorganic polymers was evaluated using scanning electron microscopy (SEM, Hitachi SU70) equipped with energy dispersion spectroscopy (Bruker EDS). Samples were coated with carbon. Crystal structure was determined by X-ray diffraction (XRD), using a PANalytical X'PERT PRO 3 instrument (Cu Kα radiation, 2.5–80°, 0.01° 2θ step-scan and 200 s/step) with phase identification by HighScore Plus software. Raman spectra were taken with a Bruker RFS 100/S spectrometer using a Nd-YAG laser (1064 nm, 350 mw) with 200 scans at a resolution of 4 cm^{-1}. UV–Vis spectra were measured by diffuse reflectance (R), and this was then converted into the absorption coefficient by the Kubelka-Munk Function, $F(R) = (1\text{-}R)^2/2R$ [32]. Wavelength in nm was also converted into eV to estimate the optical band gap energy (Eg) of the samples. Measurements were carried out on a Shimadzu UV3100 Spectrometer, over the UV–vis range (275–800 nm), with 0.02 nm step-size and using $BaSO_4$ as reference.

3. Results and discussion

Fig. 1 shows a scheme of the ecoceramic synthesis process, and an SEM image of the pyrolysed activated cork powders (in this case with HCl). In all cases the activation and pyrolysis had an effect on the overall particle size of the powders, which was now reduced to between 100 and 250 μm. The pyrolysis process has been observed previously to greatly decrease the thickness of the cell walls to ~100 nm, and to slightly increase the cell length as the slight corrugation of the cell walls found in cork is removed [24,29].

SEM images of the four differently activated pyrolysed cork powders are show in Fig. 2. It can be seen that the cork microstructure has been preserved very well in all four cases, with no discernible difference between the alkaline or acidic activators.

Raman spectra were also measured of the four activated pyrolysed cork samples, and the results are shown in Fig. 3. They all show two broad peaks centred around 1600 and 1300 cm^{-1}. This is typical of amorphous or mesoporous graphitic carbon. The G band at 1600 cm^{-1}, resulting from the C–C bond stretch in sp2 carbon [33], and which is a strong narrow peak in crystalline, well ordered graphite, becomes lower and broader when the carbon is disordered. This is accompanied by an increase in the size of the D band around 1300 cm^{-1}, which is induced by disorder, corresponding to very small graphitic domains and crystalline imperfections [34]. The ratio of the intensities of D:G can be seen as a degree of disorder in the carbon. In all of these samples, the D peak is significantly more intense than the G peak, indicating a highly amorphous and disordered carbon structure [35,36]. The ratio of the intensity of D:G is very similar for the cork activated with NaOH, HCl or HNO_3 (Fig. 3a–c), with D:G ratios of 1.42, 1.43 and 1.38, respectively. That activated with H_2SO_4 appears to be less disordered, with a D:G ratio of 1.16 (Fig. 3d). These values could all also be an indication of mesoporous carbon [37].

The pyrolysed activated cork was then infiltrated with the titania sol precursor and heated in air to produce the titania ecoceramic. SEM

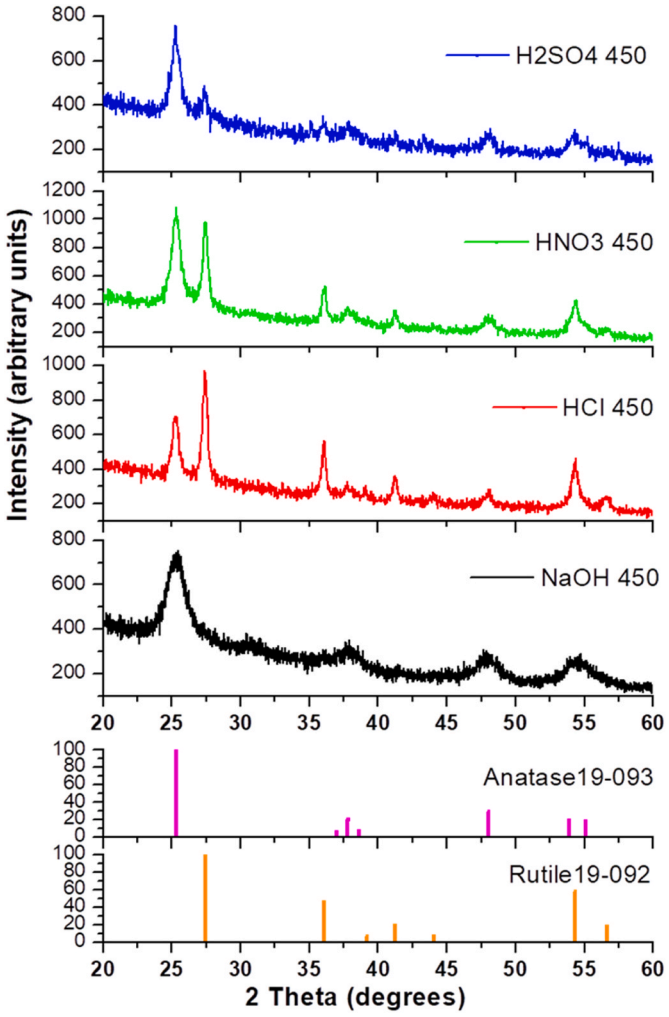

Fig. 5. XRD patterns of the TiO_2 ecoceramics heated to 450 °C, activated using NaOH, HCl, HNO_3 and H_2SO_4.

images of the TiO_2 ecoceramics heated to 450 °C are shown in Fig. 4. The sample activated with NaOH exhibits a good, biomorphic cork-like microstructure, with clearly apparent hexagonal cells ~20 μm in diameter (Fig. 4a). On the other hand, the samples activated with acids all look more "flaky", with the cork cells' walls clearly visible, but damage to the cork honeycomb cell structure (Fig. 4b–d). However, these will still be high surface area materials, even though they have lost much of their biomimetic 3-DOM nature. Unfortunately, it is almost impossible to measure the surface are of these materials due to their extremely lightweight nature and buoyancy effects from the gas flow during BET surface area measurements. The cork-like nature of the sample activated with NaOH can be better appreciated in the higher magnification image in Fig. 4e. However, the presence of residual sodium from the activation process may be an issue, especially for photocatalytic applications, as it is known that when the percentage of sodium in the titania increases, the photocatalytic activity of TiO_2 decreases as the rate of electron-hole optical recombination increases [38]. The EDS spectra of the NaOH activated ecoceramic heated to 450 °C is shown in Fig. 4f. It indicates 70.3% O, 21.4% Ti, 7.5% Na, 0.5% K and 0.4% Cl. It is well known that the accurate determination of quantities of light elements such as oxygen is unreliable by this technique, so the O value is unlikely to be accurate. Nevertheless, the ratio of Na:Ti is very high, at 1:2.85 (nearly 25% of metal ions is Na^+), and this is likely to cause major problems for photocatalysis. For this reason, the acid catalysed titania ecoceramics may be the better option for such applications.

The XRD spectra of the ecoceramics heated to 450 °C are shown in Fig. 5. In previous studies of nanopowders made from this sol-gel system heated to 450 °C/2 h, with no NaOH present, the powders consisted of 34.4 wt% anatase, 50.7 wt% rutile and 14.6 wt% brookite [30] with semiquantitative analysis, as carried out in this paper. In the NaOH activated ecoceramics, heated slowly to 450 °C, but with only a 30 min dwell, we have a virtually single phase anatase sample. This may have a small brookite peak at 30.9° (the 99.94% (2 1 1) peak), but it was too indistinct to be identified by the semiquantitative analysis. Therefore, it seems that the presence of sodium has inhibited the formation of brookite, and greatly increased the onset temperature of the anatase-to rutile transformation, as no rutile is present at all. A more detailed whole powder pattern modelling (WPPM) analysis of the sol-gel nanopowders indicated composition of 49.4 wt% anatase, 18.5 wt% brookite and only 14.8 wt% rutile after 2 h at 450 °C, with 17.3 wt% amorphous phase [31], but nevertheless, the formation of rutile has clearly been inhibited here.

With acid activation, all three ecoceramics are a mixture of anatase and rutile, but in varying ratios, and with no brookite apparent (Fig. 5). With HCl, the ecoceramic was mostly rutile (72 wt%), with anatase as a second phase (28 wt%). In studies on our titania nanoparticles made with HCl to peptise the sol, we indeed found that HCl favoured the production of rutile, resulting in a composition of 77.2 wt% rutile, 19.4 wt% anatase and just 3.4 wt% brookite after 450 °C/2 h [30]. HCl used as an activator in ecoceramic production seems to have a similar effect.

However, with HNO_3 as an activator we obtained 57 wt% anatase and 43 wt% rutile, so a surplus of nitrate ions also seems to favour the production of rutile, although less so than chloride ions. We have never studied the effects of sulphate ions, and with H_2SO_4 as the activator, anatase was the majority phase at 76 wt%, with just 24 wt% rutile. Therefore, this has a lesser effect, although still creating more rutile than observed in the previous studies on TiO_2 nanoparticles heated to 450 °C/2 h.

The UV–vis diffuse reflectance spectra of the ecoceramics heated to 450 °C are shown in Fig. 6a. All exhibit a rapid decrease in reflectivity below ~400 nm, with the acid activated ecoceramics showing an absorbance just above 400 nm, in the visible region, due to the presence of rutile. The absorption coefficient calculated by the Kubelka-Munk function, F(R), is depicted in the insert in Fig. 6a, plotted against the energy in eV. The differential of the reflectance (dR/d λ)is shown for activation with NaOH in Fig. 6b and with the acids in Fig. 6c. This is an indication of the optical band gap of the samples, Eg. As would be expected for a sample containing only anatase, the peak occurs at 382 nm, matching reported values for anatase [6]. The acid activated samples all show strong, but very noisy, peaks centred around 397–399 nm, but with a clear shoulder on the right going towards 410 nm. This is due to the intimate mixing of the anatase and rutile phases, producing a "smeared" wide band gap covering the anatase and rutile regions. The differential of the Kubelka-Munk function (dF(R)/deV) is shown in Fig. 6d and e. For the NaOH activated ecoceramic, the peak band gap Eg is indicated to be a high value of 3.39 eV (expected to be 3.23 eV), although this is an extremely broad peak. Once again, the acid activated samples have very noisy derivative plots, although all show a strong peak around 3.13 eV, midway between the values of 3.23 eV for anatase and 3.02 eV for rutile. Such results indicate that these ecoceramics merit further investigation of their photocatalytic properties under UV, visible and solar light.

To explore the effects of higher temperatures, the activated cork derived titania ecoceramics were also heated to 1000 °C. The SEM images of these samples are shown in Fig. 7. Unexpectedly, all of the samples showed more cork-like biomorphic structures, the grain growth which had occurred apparently improving this aspect of the materials. The sample activated with NaOH maintained a biomimetic cellular cork microstructure of hexagonal cells (Fig. 7a), but obvious crystallisation and grain growth had occurred. Two clear crystal types were apparent,

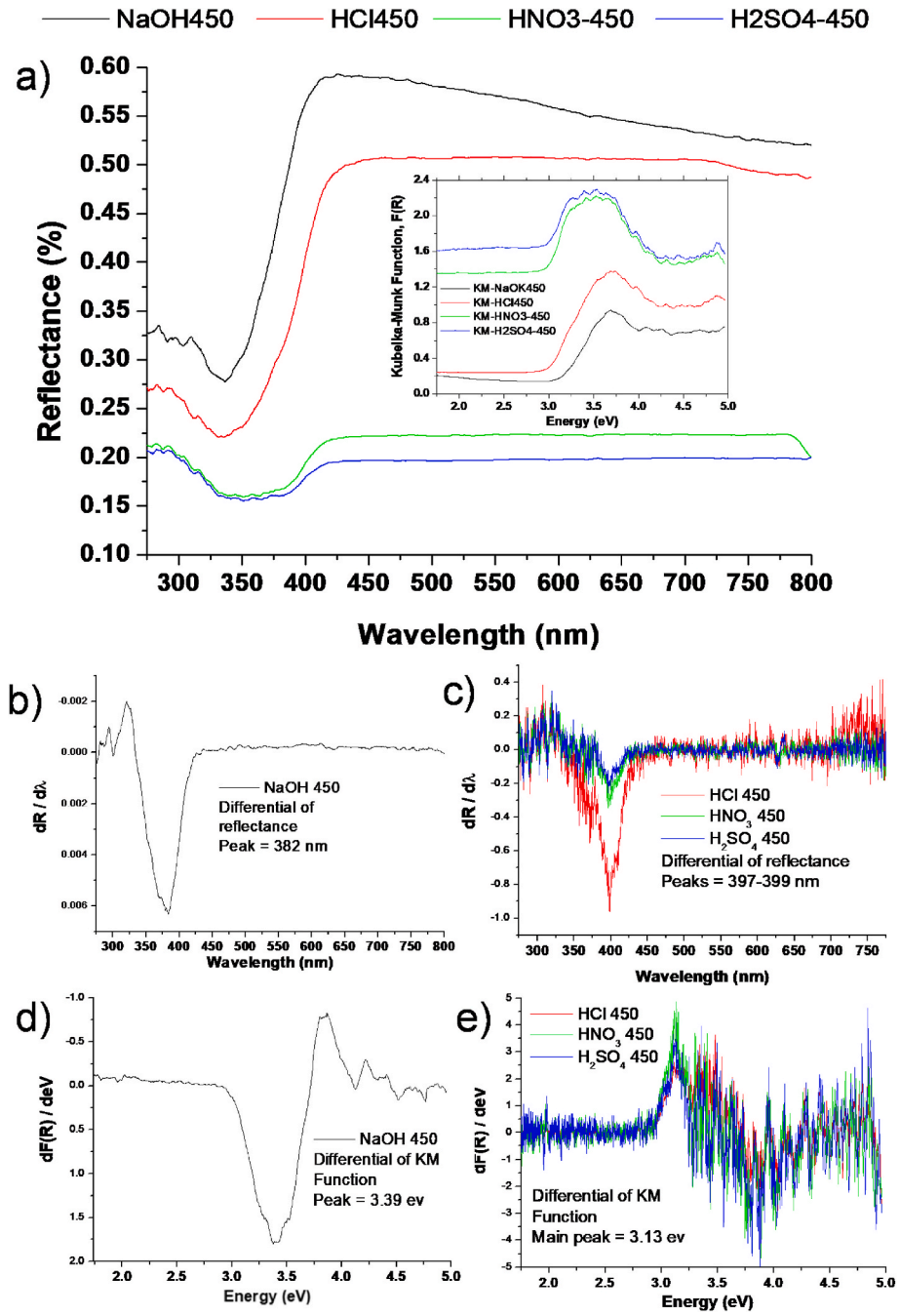

Fig. 6. a) UV–vis diffuse reflectance spectra of the TiO_2 ecoceramics heated to 450 °C, activated using NaOH, HCl, HNO_3 and H_2SO_4. The inset shows the absorption coefficent, calculated by the Kubelka-Munk function, plotted against energy, ev. The derivative of the reflectance is shown for b) NaOH and c) acid acivated ecoceramics. d) and e) show the derivative of the Kulbelka-Munk function for the NaOH and acid activated ecoceramics, respectively.

both small submicron grains and slender needles several microns long, but <1 μm in diameter. These observations will be explained by the discussion of the XRD results.

On the other hand, the samples activated with acids, despite having more cork-like cellular microstructures, look much more fragile, like lace-work – a filigree type structure (Fig. 7b–d). These consist of connected sub-micron grains with spaces between them, creating porous walls for the cells. This seems to be less so for the H_2SO_4 activated titania, which consists of more solid looking cellular structure with the "lace-work" particles decorating the end of the open cells. These clearly porous structures should result in a high surface area, if delicate, material.

The XRD spectra of the ecoceramics heated to 1000 °C are shown in Fig. 8. As would be expected at such a temperature, all of the acid activated ecoceramics consist of single phase, well crystalline rutile. However, the continuing presence of sodium in the NaOH activated titania ecoceramic has resulted in a very different material. Remarkably for TiO_2 heated to 1000 °C, it consists of anatase (20 wt%), brookite (13 wt%) and rutile (4 wt%), with the high temperature rutile phase being the most minor of these. The majority phase is a sodium titanate, $Na_2Ti_6O_{13}$, which is monoclinic with the space group C2/m. This explains the presence of the long crystalline needles observed by SEM. This accounts for 62 wt% of the ecoceramic, and demonstrates the quantity of sodium which remained in the material at 1000 °C.

Sodium hexatitanate, $Na_2Ti_6O_{13}$ is a very interesting material in its own right. It has been reported to be a photocatalyst able to split water

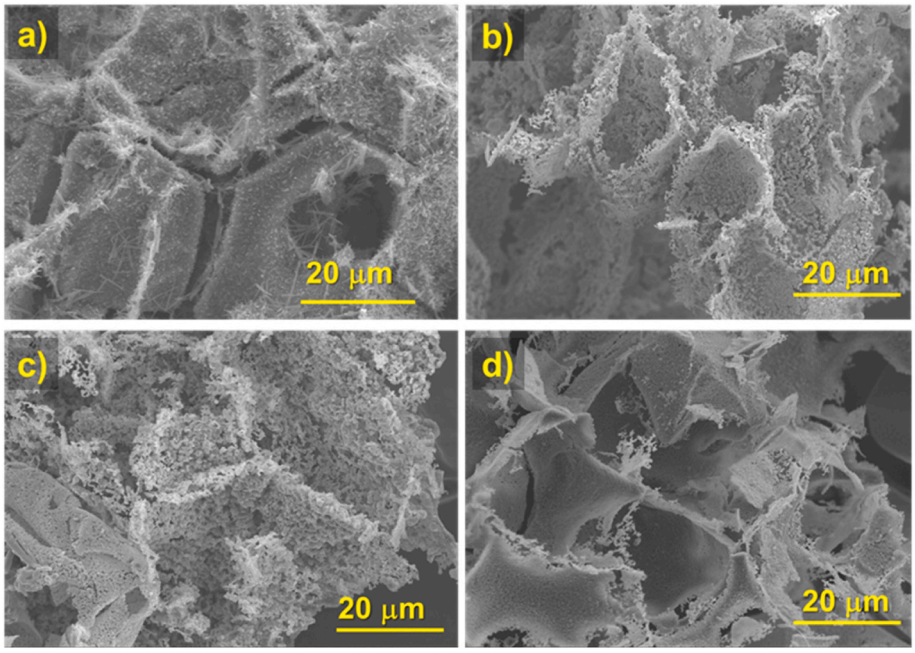

Fig. 7. SEM images of the TiO_2 ecoceramics heated to 1000 °C, activated using a) NaOH, b) HCl, c) HNO_3 and d) H_2SO_4.

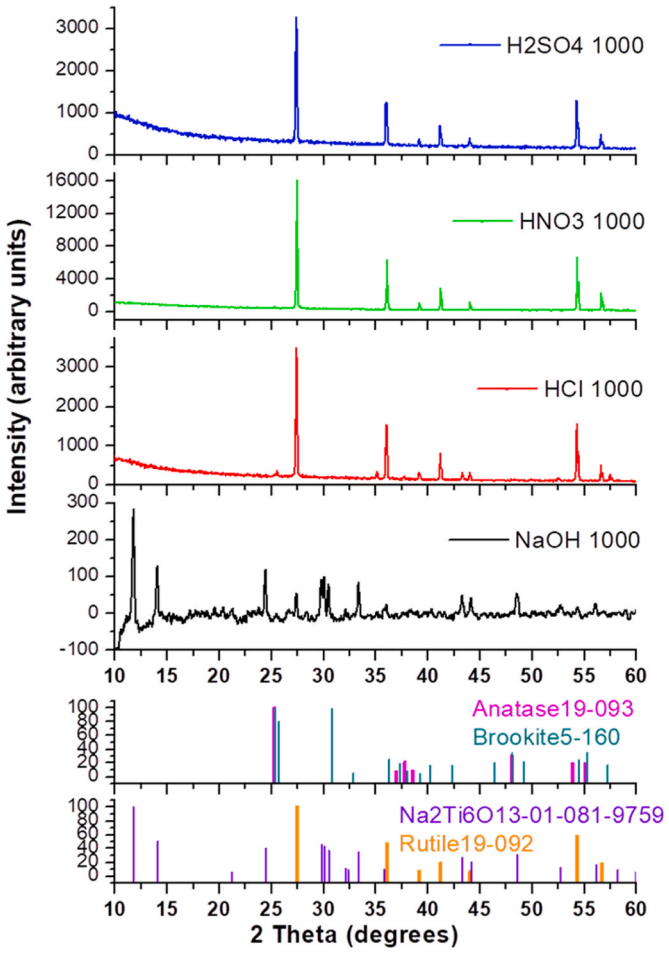

Fig. 8. XRD patterns of the TiO_2 ecoceramics heated to 450 °C, activated using NaOH, HCl, HNO_3 and H_2SO_4.

under UV light when impregnated with 0.2 wt% Ru [39]. Single crystal nanobelts of $Na_2Ti_6O_{13}$ have shown high photocatalytic efficiency of 93% after 60 min for the degradation of Rhodamine B under UV light [40]. These so-called "nanobelts" were actually 200 nm wide and in the order of ten microns long – similar to the crystalline needles observed here. These $Na_2Ti_6O_{13}$ "nanobelts" showed strong absorption in the UV region, the absorbance occurring at about 360 nm corresponding to a band gap of 3.45 eV, very close to the values also reported for $Na_2Ti_6O_{13}$ whiskers (Eg = 3.4 eV), grown at 700 °C [41]. Other $Na_2Ti_6O_{13}$ nanobelts were also reported with Eg = 3.4 eV and a 76% photodegradation efficiency in 60 min under UV [42]. $Na_2Ti_6O_{13}/TiO_2$ composite particles have also been used as photocatalysts to degrade 2,4-dichlorophenol (2,4-DCP) under a 365 nm UV lamp with a photocatalytic efficiency of 99.4% after 50 min [43]. Interestingly, visible light photocatalysts were made from $Na_2Ti_6O_{13}/TiO_2$ composite nanobelts doped with N (at 664 nm) [44], and core@shell $Na_2Ti_6O_{13}/TiO_2$ nanorods doped with S (at 664 nm) [45]. It also has potentially useful electrochemical properties for sodium ion storage batteries [40,46]. Therefore, these $Na_2Ti_6O_{13}/TiO_2$ composite ecoceramics, which appear to contain needles of similar dimensions to the "nanobelts" above, are deserving of more study and photocatalytic assessment.

The UV–vis diffuse reflectance spectra of the ecoceramics heated to 1000 °C are shown in Fig. 9a. The HCl, HNO_3 and H_2SO_4 activated ecoceramics exhibit a decrease in reflectivity in the visible spectrum, at ~410 nm, as would be expected for rutile. The NaOH activated sample has two distinct decreases, one on the edge of the visible region at ~400 nm, due to the various titania phases, and one in the UV region at ~350 nm, attributed to the $Na_2Ti_6O_{13}$. The absorption coefficient calculated by the Kubelka-Munk function, F(R), is depicted in the insert in Fig. 9a, plotted against the energy in eV, and the two different band gap energies of the NaOH activated sample can clearly be seen. The differential of the reflectance ($dR/d\lambda$) for activation with NaOH (Fig. 9b) gives the two peaks at 398 nm and 345 nm. The acid activated samples all show the expected value for rutile, ~409 nm (Fig. 9c). From the differential of the Kubelka-Munk function (dF(R)/deV), they show a slightly lower than expected Eg, between 3.07 and 3.10 eV, increasing slightly in the order HCl < HNO_3 < H_2SO_4 (Fig. 9e).

For the NaOH activated ecoceramic, the two indicated band gap energies are Eg = 3.14 eV and 3.64 eV (Fig. 9d). The first of these is what

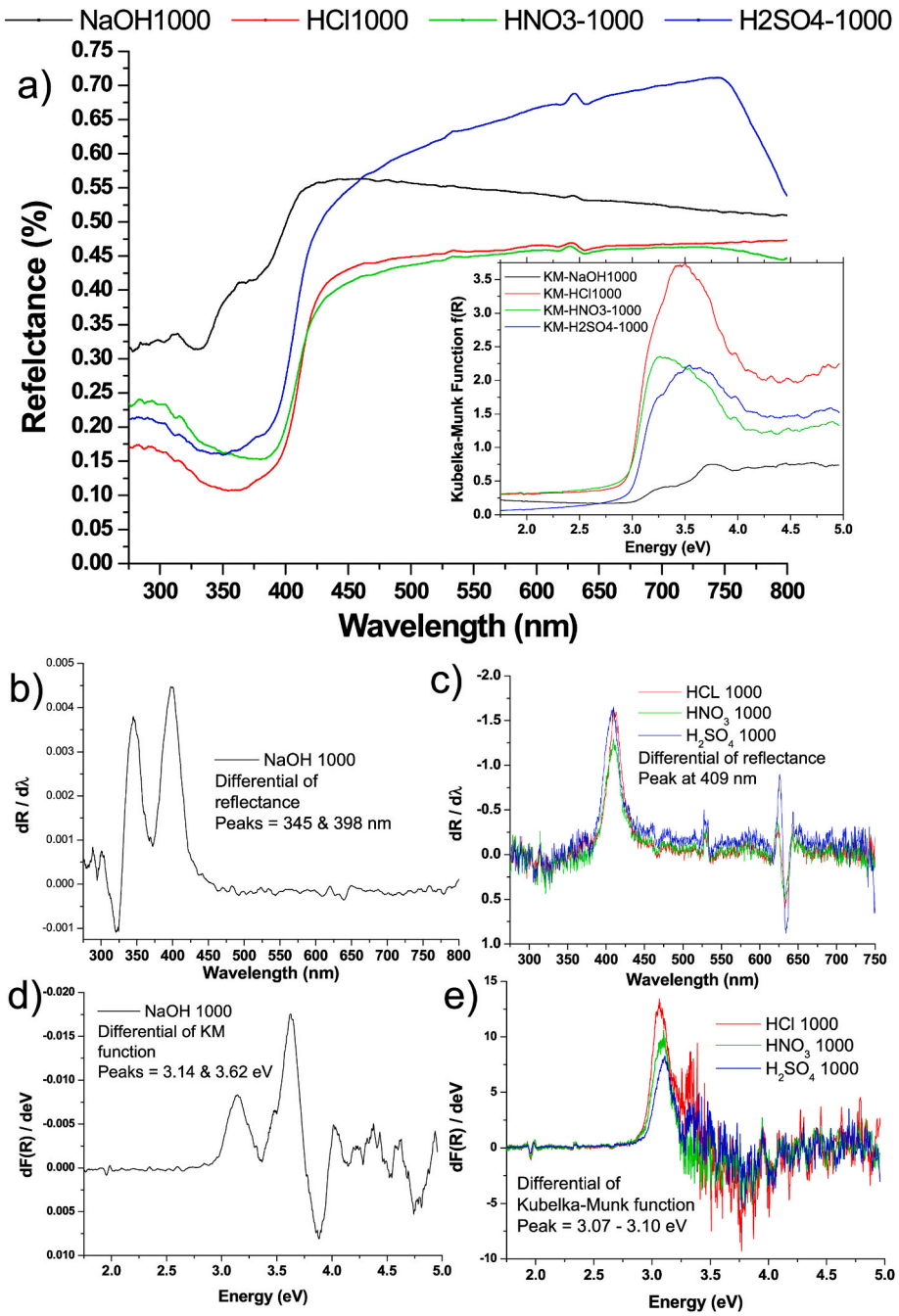

Fig. 9. a) UV–vis diffuse reflectance spectra of the TiO_2 ecoceramics heated to 450 °C, activated using NaOH, HCl, HNO_3 and H_2SO_4. The inset shows the absorption coefficent, calculated by the Kubelka-Munk function, plotted against energy, ev. The derivative of the reflectance is shown for b) NaOH and c) acid acivated ecoceramics. d) and e) show the derivative of the Kulbelka-Munk function for the NaOH and acid activated ecoceramics, respectively.

would be expected for the mixture of anatase, brookite and rutile phases, but the second is higher than expected for the reported values of $Na_2Ti_6O_{13}$, which is ~3.4 eV. Eg = 3.64 eV equates to a wavelength of 341.5 nm, which is still within the UVA region, and found in sunlight.

4. Conclusions

Ecoceramics of titania were made from sustainable cork templates for the first time. The differences between alkaline and acidic activation of the carbon template was also studied. With activation by HCl, HNO_3 or H_2SO_4, a mixture of anatase and rutile phase was formed, although these additives favoured the anatase to rutile transformation even at these low temperatures, especially for HCl. NaOH activation resulted in pure anatase, but a large amount of Na was retained in the ecoceramics. Band gaps were as expected for mixtures of such phases, in both UV and visible for anatase/rutile mixes. At 1000 °C the acid activated ecoceramics formed single phase rutile, but the NaOH activated one formed $Na_2Ti_6O_{13}$ (sodium hexatitanate) as a majority phase, coexisting with anatase, brookite and rutile. This material is worth further investigation, as $Na_2Ti_6O_{13}$ is reported as a photocatalyst in its own right.

Novel conclusions

Titania ecoceramics produced from cork were synthesised for the first time, and effects of acidic vs. alkaline activation of the cork before pyrolysis were also studied. The titania ecoceramics retained the highly

porous microstructure of the cork template in the final ceramic form. Acidic activation promoted rutile formation at only 450 °C to give mixed anatase and rutile phases, lowering the anatase-to-rutile transformation, while NaOH activation led to anatase only at 450 °C. The optical band gaps were as would be expected for anatase or anatase/rutile mixes. At 1000 °C, NaOH activation led to the formation of $Na_2Ti_6O_{13}$ coexisting with anatase, brookite and rutile, whereas the acid activated ecoceramics were pure rutile.

Declaration of competing interest

The authors declare that they have no known competing financial interests or personal relationships that could have appeared to influence the work reported in this paper.

Acknowledgements

R.C. Pullar wishes to thank FCT (Fundação para a Ciência e a Tecnologia, Portugal) grant IF/00681/2015, R.M. Novais wishes to thank FCT researcher grant Ref. CEECIND/00335/2017, and A.P.F. Caetano thanks FCT project "Bio4MURAL" PTDC/HAR-ARQ/29157/2017. This work was developed within the scope of the project CICECO-Aveiro Institute of Materials, UIDB/50011/2020 & UIDP/50011/2020, financed by national funds through the FCT/MEC and when appropriate co-financed by FEDER under the PT2020 Partnership Agreement.

References

[1] X. Chen, A. Selloni, Chem. Rev. 114 (2014) 9281–9282.
[2] A. Fujishima, K. Honda, Nature 238 (1972) 37–38.
[3] A. Fujishima, X. Zhang, D. Tryk, Surf. Sci. Rep. 63 (2008) 515–582.
[4] J. Schneider, D. Bahnemann, J. Ye, G. Li Puma, D.D. Dionysiou (Eds.), Photocatalysis, Royal Society of Chemistry, Cambridge, 2016.
[5] Z. Sen, Solar Energy Fundamentals and Modeling Techniques: Atmosphere, Environment, Climate Change, and Renewable Energy, Springer, London, 2008.
[6] M. Miyauchi, H. Irie, M. Liu, X. Qiu, H. Yu, K. Sunada, K. Hashimoto, J. Phys. Chem. Lett. 7 (2016) 75–84.
[7] T. Ohno, K. Sarukawa, M. Matsumura, J. Phys. Chem. B 105 (2001) 2417–2420.
[8] D.M. Tobaldi, R.C. Pullar, M.P. Seabra, J.A. Labrincha, Mater. Lett. 122 (2014) 345–347.
[9] P. Greil, J. Eur. Ceram. Soc. 21 (2012) 105–118.
[10] J. Martinez-Fernandez, F.M. Valera-Feria, M. Singh, Scripta Mater. 43 (2002) 813–818.
[11] M. Sing, J. Martinez-Fernandez, A.R. de Arellano-Lopez, Curr. Opt. Solid State Mater. Sci. 7 (2003) 247–254.
[12] M. Singh, B.-M. Yee, J. Eur. Ceram. Soc. 24 (2004) 209–217.
[13] P. Greil, T. Lifka, A. Kaindl, J. Eur. Ceram. Soc. 18 (1998) 1961–1973.
[14] J. Cao, O. Rusina, H. Sieber, Ceram. Int. 30 (2004) 1971–1974.
[15] S.P. Silva, M.A. Sabino, E.M. Fernandes, V.M. Correlo, L.F. Boesel, R.L. Reis, Int. Mater. Rev. 50 (2005) 345–365.
[16] A.M.A. Pintor, C.I.A. Ferreira, J.C. Pereira, P. Correia, S.P. Silva, V.J.P. Vilar, C.M. S. Botelh, R.A.R. Boaventura, Water Res. 46 (2012) 3152–3166.
[17] H. Pereira, Cork: Biology, Production and Uses, Elsevier B.V, Amsterdam, 2007.
[18] L. Gil, Cortiça: Produção, tecnologia e aplicação, INETI, Lisbon, Portugal, 1998.
[19] http://www.saomarcosdaserra.com/cork.php. Jan 2020.
[20] R.C. Pullar, P. Marques, J. Amaral, J.A. Labrincha, Mater. Des. 82 (2015) 297–303.
[21] R.C. Pullar, R.M. Novais, Mater. Today 20 (2017) 45–46.
[22] A. Quarta, R.M. Novais, S. Bettini, M. Iafisco, R.C. Pullar, C. Piccirillo, J. Environ. Chem. Eng. 7 (2019) 102936.
[23] F. Scalera, L. Carbone, S. Bettini, R.C. Pullar, C. Piccirillo, J. Environ. Chem. Eng. 8 (2020) 103594.
[24] R.M. Novais, R.C. Pullar, J. Eur. Ceram. Soc. 39 (2019) 1287–1296.
[25] F.A. Costa Oliveira, M.A. Barreiros, A. Haeussler, A.P.F. Caetano, A.I. Mouquinho, P.M. Oliveira e Silva, R.M. Novais, R.C. Pullar, S. Abanades, Sustain. Energy Fuels 4 (2020) 3077–3089.
[26] F.C. Oliveira, M.A. Barreiros, S. Abanades, A.P.F. Caetano, R.M. Novais, R. C. Pullar, *J. CO_2 Util.* 26 (2018) 552–563.
[27] D.M. Tobaldi, R.C. Pullar, A.F. Gualtieri, M.P. Seabra, J.A. Labrincha, Chem. Eng. J. 214 (2013) 364–375.
[28] MF5 Cork Granules, Specification Sheet PDA 1023/9, Amorim Cork Composites.
[29] R.M. Novais, A.P.F. Caetano, M.P. Seabra, J.A. Labrincha, R.C. Pullar, J. Clean. Prod. 197 (2018) 1137–1147.
[30] D.M. Tobaldi, R.C. Pullar, R. Binions, A. Belen-Jorge-Sobrido, P.F. McMillan, M. Saeli, M.P. Seabra, J.A. Labrincha, Catal. Sci. Technol. 4 (2014) 2134–2146.
[31] D.M. Tobaldi, R.C. Pullar, A.F. Gualtieri, A. Belen Jorge, R. Binions, P.F. McMillan, M.P. Seabra, J.A. Labrincha, CrystEngComm 17 (2015) 1813–1825.
[32] A.S. Marfunin, Physics of Minerals and Inorganic Materials. An Introduction, Springer-Verlag, Berlin, 1979.
[33] K. Krishnamoorthy, M. Veerapandian, R. Mohan, S. Kim, Appl. Phys. Mater. Sci. Process 106 (2012) 501–506.
[34] M. Marton, M. Vojs, E. Zdravecká, M. Himmerlich, T. Haensel, S. Krischok, M. Kotlár, P. Michniak, M. Veselý, R. Redhammer, J. Spectroscopy 2013 (2013) 467079.
[35] S. Perumbilavil, P. Sankar, T.P. Rose, R. Philip, Appl. Phys. Lett. 107 (2015), 051104.
[36] F. Tuinstra, J.L. Koenig, J. Chem. Phys. 53 (1970) 1126–1130.
[37] J.-G. Li, C.-Y. Tsai, S.-W. Kuo, Polymers 6 (2014) 1794–1809.
[38] C. Hou, B. Hu, J. Zhu, Catalysts 8 (2018) 575.
[39] Y. Inoue, T. Kubokawa, K. Sato, J. Chem. Soc., Chem. Commun. 1990 (1990) 1298–1299.
[40] X.K. Zhang, J.J. Yuan, H.J. Yu, X.R. Zhu, Z. Yin, H. Shen, Y.M. Xie, J. Alloys Compd. 631 (2015) 171–177.
[41] K. Teshima, S. Lee, S. Murakoshi, S. Suzuki, K. Yubuta, T. Shishido, M. Endo, S. Oishi, Eur. *J. Inorg. Chem.* 2010 (2010) 2936–2940.
[42] L. Zhen, C. Xu, W. Wang, C. Lao, Q. Kuang, Appl. Surf. Sci. 255 (2009) 4149–4152.
[43] Z. Jian, S. Huang, Y. Zhang, Int. J. Photoenergy 2013 (2013) 606291.
[44] C. Liu, T. Sun, L. Wu, J. Liang, Q. Huang, J. Chen, W. Hou, Appl. Catal., B 170–171 (2015) 17–24.
[45] C. Liu, J. Liang, R. Han, Y. Wang, J. Zhao, Q. Huang, J. Chen, W. Hou, Phys. Chem. Chem. Phys. 17 (2015) 15165–15172.
[46] C. Ho, C. Ying, V. Li, K.-Y. Chan, Ind. Eng. Chem. Res. 55 (2016) 10065–10072.